PAPER

Check for updates

Synthesis of a novel hydrazone-based compound applied as a fluorescence turn-on chemosensor for iron(III) and a colorimetric sensor for copper(II) with antimicrobial, DFT and molecular docking studies†

Sharmin Akther Rupa,[a] Md Abdul Majed Patwary, [ID] *[a] William Emmanuel Ghann,[b] Adams Abdullahi,[b] A. K. M. Royhan Uddin,[a] Md. Mayez Mahmud,[c] Md. Aminul Haque,[d] Jamal Uddin [ID] [b] and Mohsin Kazi[e]

Hydrazone–hydrazide-based linkers perform a crucial role in environmental as well as biological fields. Such linkers are employed to detect exact metal ions at a minute level; hence, numerous probes are available. Even though thiophene-based molecules have a unique position in the medicinal arena, only very few chemosensors are reported based on such a moiety. In this current work, a novel hydrazide–hydrazone-based fluorogenic molecule 5-bromo-2-hydroxy-N'-[(1E)-1-(thiophen-2-yl)ethylidene]benzohydrazide (L) has been successfully designed and synthesized. The sensing studies of L demonstrated a ratio metric as well as turn-on-enhanced fluorescence and colorimetric response toward Fe^{3+} and Cu^{2+} ions, respectively and it was observed to be insensitive toward various metal ions. The Job plots revealed that the binding stoichiometry of L and metal ions is 2 : 1. In addition, density functional theory (DFT) results strongly suggested that L can be used as a powerful colorimetric sensor for the detection of Cu^{2+} ions. *In vitro* antimicrobial activities of L were evaluated by disk diffusion and results revealed good antibacterial activities against *E. coli*. Further, molecular docking was executed with DNA gyrase (PDB ID: 1KZN) of *E. coli* and the calculated interaction energy value was found to be -7.7 kcal mol^{-1}. Finally, molecular docking, fluorescence, colorimetry and the HOMO–LUMO energy gap of the compound can provide new insights into developing drugs and detecting metals in biomolecules.

1. Introduction

Hydrazide–hydrazones are a unique category of Schiff base compounds containing the –CO–NHN═CH– functional group. Due to various medicinal properties such as antibacterial, antiviral, antifungal, anticancer and anti-inflammatory activities, such compounds have attracted substantial interest over many years in the design of novel chemical compounds.[1–7] Moussa and co-workers reported a series of organic compounds containing the hydrazone moiety, which demonstrated high antioxidant activity against tyrosinase and cholinesterase.[8]

[a]Department of Chemistry, Comilla University, Cumilla-3506, Bangladesh. E-mail: mamajedp@gmail.com

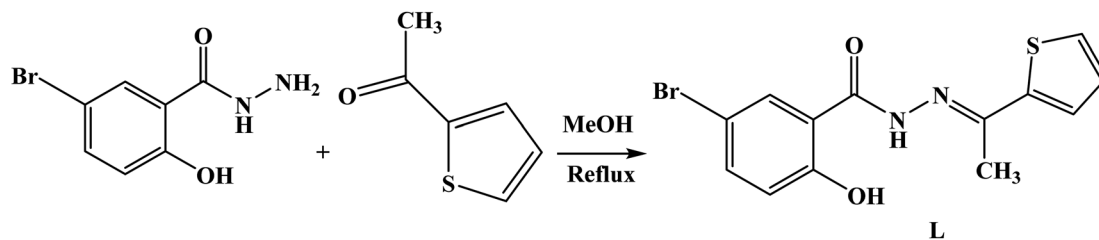*[b]Center for Nanotechnology, Department of Natural Sciences, Coppin State University, Baltimore, USA*

[c]Tokushima University, Faculty of Pharmaceutical Science, Tokushima Shi 770-0026, Japan

[d]Department of Chemistry, Jagannath University, Dhaka-1100, Bangladesh

[e]Department of Pharmaceutics, College of Pharmacy, King Saud University, P.O. Box 2457, Riyadh 11451, Saudi Arabia

† Electronic supplementary information (ESI) available. See DOI: https://doi.org/10.1039/d3ra04364a

Rahim *et al.* designed and synthesized an aromatic hydrazide-based Schiff base targeting Alzheimer's disease that was shown to significantly inhibit acetylcholinesterase and butyrylcholinesterase compared to the standard physostigmine.[9]

Moreover, chemosensors containing hydrazone–hydrazide moieties are considered potential candidates due to their high sensitivity and selectivity for detecting several cations and anions.[10] Fluorescent sensors have attracted extensive attention from researchers in the past few decades owing to their operational simplicity, high sensitivity, extreme selectivity, low instrumental cost, nondestructive sample analysis, *etc.*[11] The signal of a fluorescent sensor is usually monitored as a change in its emission intensity, fluorescence lifetime, or a shift of emission wavelength to subtle environmental changes. On the other hand, the development of highly selective ratio metric and "turn-on" fluorescent probes have superior significance due to their capability of detecting metal ions even in living systems, which was found to display different emission behavior upon metal binding.[12,13]

Iron is one of the most abundant metals in the human body as well as in the Earth's crust.[14] It plays a ubiquitous role in many biochemical processes of plants and animals including oxygen

Scheme 1   Synthesis of L from 5-bromo-2-hydroxybenzohydrazide and 2-acetylthiophene in MeOH.

transport, cellular metabolism, electron transfer and serves as an active site in myoglobin, hemoglobin, siderophores, and cytochromes.[15] Especially, ferric ion (Fe^{3+}) is responsible either for structural purposes or as part of a catalytic site in many proteins, lipids and enzymes.[16] The deficiency of iron will lead to low oxygen delivery to cells, resulting in anemia, hemochromatosis, liver/kidney damage, diabetes, and cancer.[17] Equally, excess iron in a living cell is considered a biohazard as it is prone to produce reactive oxygen species (ROS) through Fenton-reaction, which induces several serious diseases, such as Alzheimer's, Huntington's, and Parkinson's diseases.[18] On the other hand, Cu^{2+} is the third most essential transition metal in the human body, which plays several important roles, for example, iron absorption, maintaining nerves, and blood vessels.[19] Moreover, it acts as a catalytical co-factor in several metalloenzymes, for instance, superoxide dismutase, cytochrome c oxidase, and tyrosinase.[20] However, the abnormal level of copper intake also causes destructive consequences to the body (WHO >2 ppm), such as irritation of the nose and throat, nausea, vomiting, and diarrhoea.[21,22] On the contrary, copper deficiency in the human body leads to abnormal growth of bones. It turns toxic due to accumulation in cell membranes that lead to the disorder of cellular homeostasis, which causes oxidative stress accompanied by several neurodegenerative syndromes, ranging from Menkes, Wilson, hallucinations, depression, familial amyotrophic lateral sclerosis, schizophrenia, and Alzheimer's.[23,24] Hence, the design and synthesis of new chromo-fluorogenic sensors for the detection of metals through simple synthetic mechanisms are of considerable importance for the environment and human health.

Therefore, the present study was designed to synthesize hydrazide–hydrazone-based compound **L** derived from the coupling of aromatic ketone and phenolic acids hydrazides containing bromo and hydroxyl groups. **L** possesses a tridentate –ONS– binding pocket (Scheme 1). Density functional theory (DFT) calculations were performed to check the geometrical and electronic structural features of **L**, Fe^{3+} and Cu^{2+} complexes. In addition to that, **L** was tested *in vitro* antimicrobial study against some Gram-negative, Gram-positive bacteria, and the fungus strain showed moderate inhibitory results. Finally, molecular docking methodology was used to study the molecular behavior of **L** with *E. coli* to identify their binding interactions.

2.   Experimental data

All chemicals were purchased from Sigma-Aldrich and used as received without further purification. Infrared (IR) spectra were recorded on a Shimadzu (FTIR) Prestige-21 spectrophotometer (range: 4000–400 cm^{-1}, using KBr disk), ^{1}H, and ^{13}C NMR spectra were recorded on a Bruker DPX-400 spectrophotometer using tetramethyl silane as an internal reference. NMR spectra were recorded on dimethyl sulfoxide (DMSO) solvent. Mass spectra were obtained from VG Micro mass 7070HS (EI) and HP1100MSD (LCMS) spectrometers. Steady-state fluorescence spectra were recorded on a HORIBA NanoLog spectrofluorometer. Time-correlated single photon counting (TCSPC) measurements using a HORIBA-Deltaflex were conducted for fluorescence lifetime measurements.

2.1.   Synthesis of L

The synthetic procedure for the new sensor is described as follows. A solution of 5-bromo-2-hydroxybenzohydrazide (0.5 g, 3 mmol) in methanol (20 mL) was added to a solution of 2-acetyl thiophene (0.83 g, 2 mmol) in methanol (10 mL) with continuous stirring. The resulting mixtures were stirred at 60 °C over a period of 6 hours (Scheme 1). A yellow precipitate was formed during the reaction which was collected by filtration and dried under a vacuum. Yield: 47% mp: >240 °C. IR (KBr, cm^{-1}) (Fig. S1†): ν 3477s (–OH), 3290s (–NH), 1637s (–C=O), 1599s (–C=N), 956s (–N–N). ^{1}H NMR (DMSO, 400 MHz) (Fig. S2†): δ 12.11 (s, H, phenolic OH), 11.25 (s, H, NH), 8.03 (s, H, H–phenyl), 7.65 (d, H, J = 2.4 Hz, H–phenyl), 7.59 (d, H, J = 2.0 Hz, H–phenyl), 7.57 (d, H, J = 2.8 Hz, H–thiophene), 7.13 (dd, H, J = 3.2 Hz, H–thiophene), 7.00 (d, H, J = 5.8 Hz, H–thiophene), 2.37 (s, 3H, H–methyl). ^{13}C NMR (DMSO, 100 MHz) (Fig. S3†): δ 176.86, 160.85, 156.31, 143.34, 136.11, 132.87, 129.68, 128.94, 128.09, 120.62, 119.78, 108.09, 14.75. ESI-MS: calculated for $[\mathbf{L}]^+$ (Fig. S4†): *m/z* 337.9725. Found: *m/z* 337.9712.

2.2.   Antimicrobial activity assay

In vitro antimicrobial action of compound **L** was assessed by agar disc diffusion technique.[1] Mueller Hinton Agar (MHA) media was utilized as a control for bacteria analysis and Potato Dextrose Agar (PDA) media was utilized for fungal strain as already discussed and reported earlier.[1] After preparation, the MHA and PDA media were nurtured for a day, and contaminations were tested. The test organism was inoculated by means of the sterile cotton bar on media after incubation. The sample discs were kept for 1 day for antibacterial assay at 37 °C and for 2 days at 26 °C for antifungal assay on pre-inoculated agar plates and aerobically incubated. DMSO was employed as a control. Each disc was introduced with 50 μL of the sample in

DMSO having 300 μg of the synthesized compound, **L**. 50 μg per disc for the standard ceftriaxone and amphotericin B solutions in DMSO were loaded per disc for antibacterial and antifungal assays as a positive control, respectively. The diameter of the zone of inhibition (ZOI) in mm circling of the disc was assessed after the timely incubation for antibacterial and antifungal assay. In this research, two Gram-positive *Staphylococcus aureus* (cars-2) and *Bacillus megaterium* (BTCC-18), two Gram-negative *Escherichia coli* (carsgn-2) and *Salmonella typhi* (JCM-1652) bacteria, as well as two fungal strains *Trichoderma harzianum* (carsm-2) and *Aspergillus niger* (carsm-3) were utilized.

2.3. Protein–ligand docking

The 3D crystal structure of *E. coli* (PDB ID: 1KZN) was obtained in pdb format from the online protein data bank (PDB) database. The structure was verified, and energy minimization was performed with the Swiss-Pdb Viewer software packages (version 4.1.0),[25] since the crystal structure contains a variety of issues related to improper bond order, side chains geometry, and missing hydrogen atoms. Prior to docking, all the hetero-atoms and water molecules were removed from the crystal structure using PyMol (version 1.3) software packages.[26] Both the structures of the proteins and ligands were saved in .pdbqt format by PyRx 0.8 for docking analysis.[27] The grid box that encloses amino acids domain involved in the binding active sites, had the dimension of $25 \times 25 \times 25$ Å^3 (x × y × z) and center of $19.53 \times 19.16 \times 43.28$ Å^3 (x × y × z). The docked conformation of the respective protein conformer with the lowest binding free energy was analyzed using PyMOL Molecular Graphics System (version 1.7.4) and Accelrys Discovery Studio 4.1.[28]

3. Results and discussion

3.1. Colorimetric analysis of Cu^{2+}

The recognition profiles of **L** (10 μM) toward different metal cations (1 eq.) were also investigated by absorption spectroscopy. The selectivity of **L** towards various cations Cr^{3+}, Mn^{2+}, Pb^{2+}, Fe^{2+}, Fe^{3+}, Co^{2+}, Ni^{2+}, Cu^{2+}, Zn^{2+}, Na$^+$, K$^+$, Mg^{2+}, Ca^{2+}, and Al^{3+} was achieved in DMSO as demonstrated in Fig. 1. When an equivalent amount of the cations was added to the **L**, only Cu^{2+} enhanced significantly produced an intensive color change, while the rest of the metal ion solutions showed a very mild alteration or almost no change in color. Hence, the combination of the ligand with copper ions was further investigated by spectroscopic and theoretical means. The UV-vis absorption spectra of the ligand in DMSO showed an absorbance maximum at 330 nm due to a symmetry-allowed $\pi \rightarrow \pi^*$ transition rather than a symmetry-forbidden $n \rightarrow \pi^*$ transition. In addition, two isosbestic points were observed at 290 and 346 nm in the colorimetric titration of the ligand with Cu^{2+} as shown in Fig. 2, which clearly indicates the smooth molecular conversion of free ligand to metal complex. The detection limit of **L** toward Cu^{2+} was obtained using the calibration curve of absorbance *versus* concentration, which was found to be as low as 2.35 μM.

3.2. Fluorescence detection of Fe^{3+}

Fig. 3 illustrates the fluorescent alterations of **L** (10 μM) with diverse cations (1.0 equiv.) with an excitation at 360 nm whereas, the inset shows a comparison of UV-vis spectra of **L** (10 μM) before and after addition of Fe^{3+}. As evident from Fig. 4, the DMSO solution of **L** (10 μM) shows fluorescence emission at 455 nm when excited at 360 nm. Upon the addition of 1 eq. of Fe^{3+}, a new significant broad fluorescence emission at about
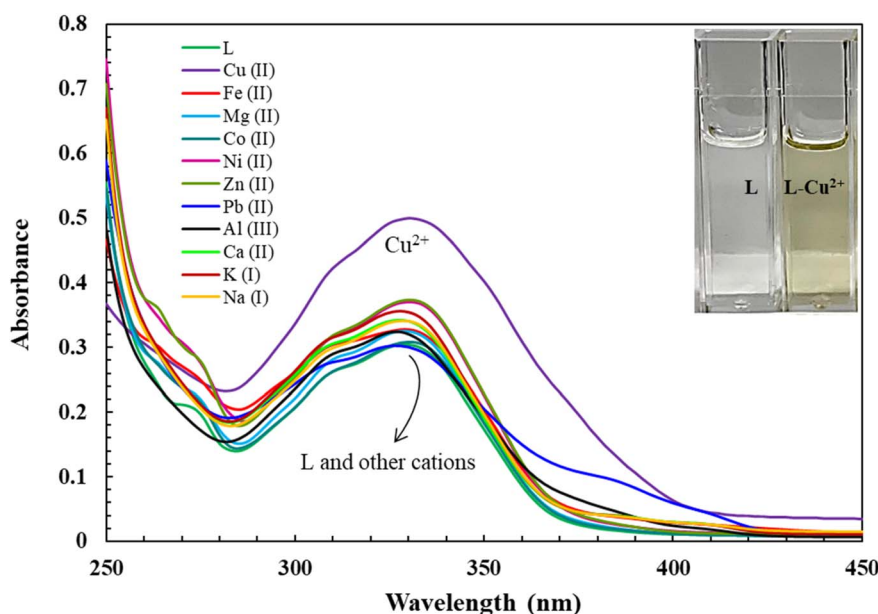

Fig. 1   Absorbance *vs.* wavelength (nm) of ligand **L** (10 μM) with equivalent addition of different metal ions in DMSO. Inset: visual color changes of **L** and **L**-Cu^{2+} under daylight.
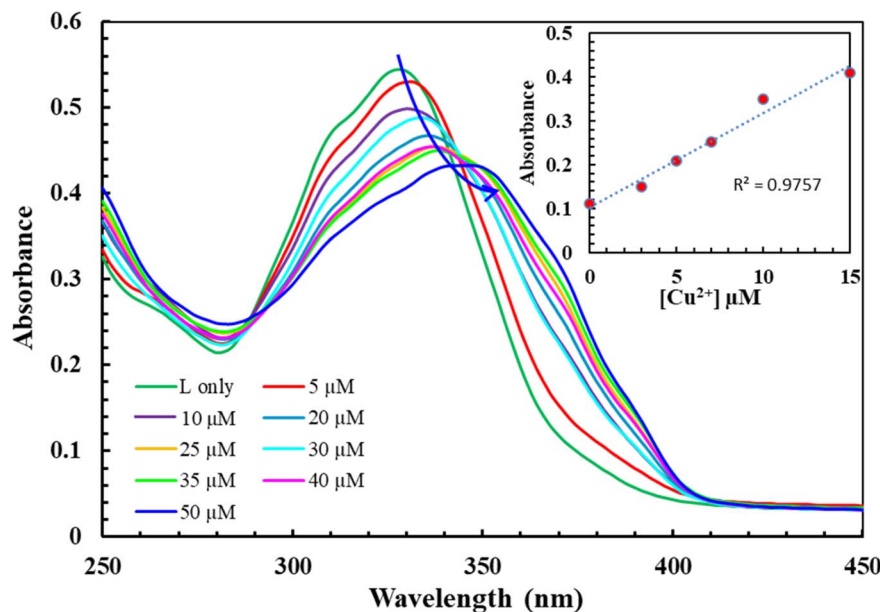
Fig. 2 Absorbance *vs.* wavelength (nm) of **L** (10 μM) in the presence of varying concentration of Cu^{2+} (0–100 μM) in DMSO. Inset: detection limit of **L** (10 μM) towards Cu^{2+} based on 3σ/slope at 346 nm using UV-visible titration experiment.

550 nm was clearly observed, whereas Cr^{3+}, Mn^{2+}, Pb^{2+}, Fe^{2+}, Fe^{3+}, Co^{2+}, Ni^{2+}, Cu^{2+}, Zn^{2+}, Na^+, K^+, Mg^{2+}, Ca^{2+}, Al^{3+} and Bi^{2+} showed no emission band at this wavelength. These results indicated that **L** could function as a fluorescent "turn-on" type sensor for Fe^{3+} ions. It can be assumed that the emergence of the new fluorescence emission might demonstrate the coordination process of Fe^{3+} with **L**, which is also supported by the generation of a new absorption band at 355 nm in the UV-vis spectrum of **L** + Fe^{3+} when compared with that of **L** (Fig. 4; Inset). In addition, the remarkable stokes shift ($\lambda_{em} - \lambda_{abs/ex} = 195$ nm) of **L** + Fe^{3+} enables the clear separation of the excitation

and emission bands, which is highly desirable for the fluorescent detection of metals. For better investigation, we have carried out the fluorescence titration of **L** with the subsequent addition of Fe^{3+} and found that the emission intensity at 550 nm gradually increased. The ratio metric and fluorescence enhancement of **L** witnessed the visual detection of Fe^{3+} ions when the samples were exposed to a UV lamp. The quantum yields of **L** increased from 0.0019 to 0.052 upon binding of Fe^{3+}. Accordingly, **L** could be utilized as an excellent turn-on fluorescence chemoreceptor for Fe^{3+} ions (Fig. 4). The detection limit of **L** toward Fe^{3+} was obtained using the calibration curve
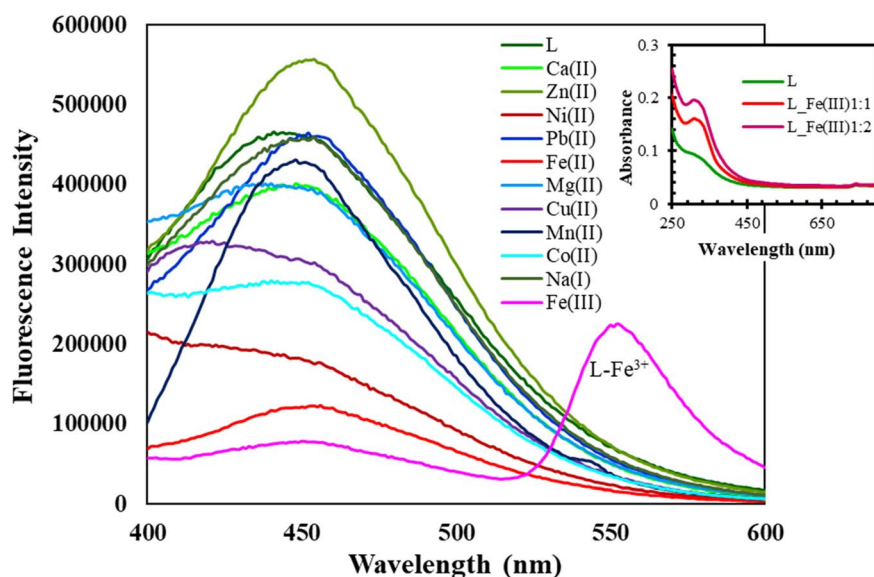

Fig. 3 Fluorescent variations of **L** (10 μM) with various cations (1.0 equiv.) with an excitation at 360 nm; inset: comparison of UV-vis spectra of **L** (10 μM) before and after addition of Fe^{3+}.
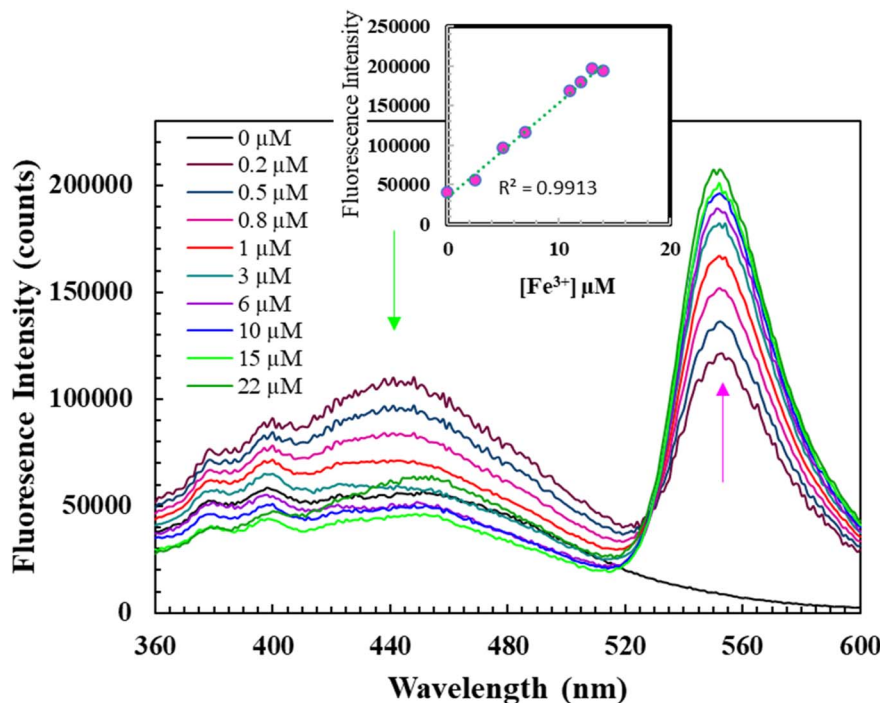
Fig. 4 Fluorescence spectra of **L** (10 μM) (λ_{ex} = 360 nm) with varying concentrations of Fe^{3+} in DMSO; insets: detection limit of **L** (10 μM) towards Fe^{3+} based on 3σ/slope at 550 nm using fluorometric titration experiment.

of emission *versus* composition, which is an important factor for a better sensor. According to the U.S. EPA regulations, it should be less than the limit of ~20 μM or less.[29] The detection limit of **L** toward Fe^{3+} ions was found to be as low as 3.87 μM.

The photophysical properties of **L** were studied using time-resolved emission experiments in the absence and presence of Fe^{3+}. Lifetime experiments for the chemosensors **L** and its Fe^{3+} complex was studied at 298 K in DMSO solvent. The values of fluorescence lifetime of **L** and **L** + Fe^{3+} are 3.46, and 6.57 ns, respectively as represented in Fig. 5. Both **L** and its complex

showed a bi-exponential decay, which may be due to the formation of different hydrogen-bonded species in highly polar DMSO solvents.[30]

3.3. Interaction mode and sensing mechanism

To find out the interaction mode of Fe^{3+} and Cu^{2+} with **L**, the Job's plot and FT-IR were employed. The stoichiometric ratio between Fe^{3+} and Cu^{2+} with **L** was established through the continuous variation method. From Job's plot, it is evident that the ratio between the ratio of Fe^{3+} and Cu^{2+} with **L** was 1 : 2 (see ESI Fig. S5 and S6†). To understand the binding sites between them further, IR spectra were recorded in KBr as shown in Fig. 6. From the IR spectra of **L**, **L** + Cu^{2+} and **L** + Fe^{3+}, it is distinct that the stretching vibration band of –C=O (1637 cm^{-1}) disappeared with the addition of metals (Fig. 6). This suggested that the coordination has taken place through an oxygen atom of C=O group. At the same time, shifting of –C=N stretching vibration peak to lower wave number in the complex from 1599 to 1586 cm^{-1} suggested the involvement of azomethane nitrogen in bonding.[31] The bands at 3400–3600 cm^{-1} in **L**, Cu^{2+} and Fe^{3+} complexes, are assigned to phenolic–OH.[32]

Fig. 7 illustrates the possible binding mode for **L** in upon addition of Fe^{3+} and Cu^{2+}. It seems that Fe^{3+} and Cu^{2+} adopts a coordination mode with nitrogen atoms (–C=N) of the receptor **L**, that inhibits the non-radiative transitions such as –C=N isomerization. The –C=N isomerization inhibition process induced by the Fe^{3+} binding warrants the chelation-induced enhanced fluorescence (CHEF) effect.[33] Thus, the fluorescence enhancement of **L** upon binding to Fe^{3+} might be due to CHEF effect.
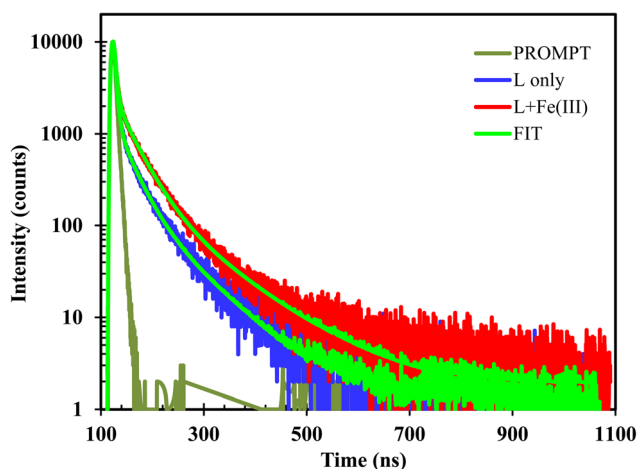

Fig. 5 Excited state fluorescence decay behavior of **L** and complexes with Fe^{3+} (10 μM) in DMSO solvent at room temperature (excitation wavelength: 400 nm).

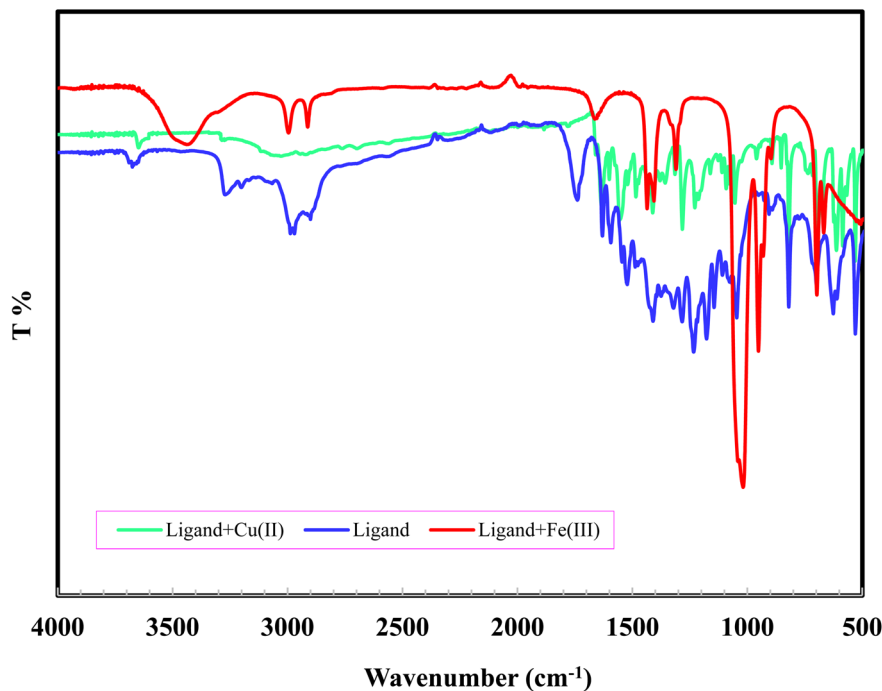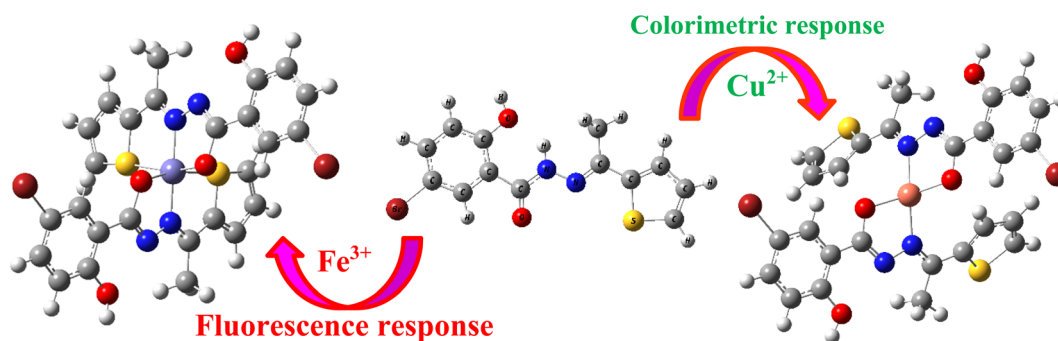**Fig. 6** FT-IR spectra of **L** and, its Fe^{3+} and Cu^{2+} complexes recorded in KBr.

Fig. 7 Plausible binding mode for **L** in upon addition of Fe^{3+} and Cu^{2+}.

3.4. Application of L in water sample

To test the reliability of **L** in a real sample with Cu^{2+} ion, it was employed to detect concentration of Cu^{2+} in tap water samples. In order to verify the accuracy of the established procedure, recovery experiments were carried out by spiking the tap water samples with different concentrations of Cu^{2+} and **L** in DMSO (2 mL) before any pretreatment.[34] The change in absorbance of **L** with the above water samples was tested by adding 20, 40, and 80 μM of Cu^{2+} individually. Each sample was analyzed three times in H_2O/DMSO (v/v, 8/2). The results are tabulated in Table 1. The results suggest that sensor **L** can be used in real test samples.

3.5. Antimicrobial study

In vitro sensitivities of two Gram-positive and two Gram-negative bacteria including two fungal strains against the synthesized compound were assessed by agar disc diffusion technique.[1,35] The formation of the diameter of ZOIs in mm by the synthesized analogue is shown in Table 2. Compound **L** demonstrated moderate activity against *E. coli* bacteria compared to other bacterial and fungal strains. The outcomes represented in Table 2 point out that **L** had better antibacterial activity against *E. coli*, with a mean ZOI of 12 mm diameter at 300 μg mL^{-1}. While, **L** had a low mean ZOI for *T. harziana*, and *A. niger*, suggesting that had a low antifungal activity effect.

Table 1 Application of L for the determination of Cu^{2+} concentrations in tap water samples

Sample	Added Cu^{2+} (μM)	Found (μM)	Recovery (%)	RSD (%) ($n = 3$)
Tap water	20	15.4	77	1.3
	40	31.6	79	1.2
	80	61.1	76	1.5

Table 2 Diameter of inhibition zones (mm) of the synthesized compounds ceftriaxone, and amphotericin B against tested bacterial and fungal strains

Compounds	Gram (+) bacteria		Gram (−) bacteria		Fungi	
	S. aureus	*B. megatherium*	*E. coli*	*S. typhi*	*T. harzianum*	*A. niger*
L	9	9	12	10	7	6
Ceftriaxone	40	50	38	44	—	—
Amphotericin B	—	—	—	—	8	17
DMSO	—	—	—	—	—	—

3.6. Molecular docking analysis

Molecular docking, a subfield of computational chemistry and bioscience, is a powerful tool to investigate and provide several quick insights into ligand–receptor interactions in order to facilitate the design of potential drugs.[36,37]

To investigate and compare the antimicrobial activity of the synthesized compound with experimental data, a docking analysis of **L** against *E. coli* was performed. Thus, to get the binding conformations of these compounds, **L** was docked in the active site of *E. coli* DNA Gyrase (PDB ID: 1KZN) using the PyRx 0.8. The most stable anchoring conformations of these compounds along with interacting residues are shown in Fig. 8 created with the help of the discovery studio visualizer.[29]

The binding energies for **L** with 1KZN were −7.7 kcal mol^{-1}, whereas the binding energy for Ciprofloxacin was reported −9.2 kcal mol^{-1}.[38] In **L**-1KZN, **L** formed two conventional hydrogen bonds (2.63 and 3.00 Å) of O–H⋯O–C with active site residues GLU50 and THR165. Pi-anion, pi-sigma and pi-alkyl bonds were also noticed with GLU50 (4.23 Å), VAL43 (4.62 Å), ALA47 (5.43 Å), VAL71 (5.47 Å), ILE78 (5.07 Å), VAL167 (5.06 Å), PRO79 (4.82 Å), and THR165 (3.75 Å) respectively. It was also noted that an electrostatic bond was found between N and residue ASP73 as shown in Fig. 8. Results of docking studies revealed that **L** formed bonds to the active site of 1KZN and showed strong interactions with GLU50, THR165, and ASP73 of DNA gyrase enzyme (PDB ID: 1KZN) as shown in Fig. 9, which also supports the literature.[20,39] Thus, computational results are in good agreement with *in vitro* experimental data (Table 3).
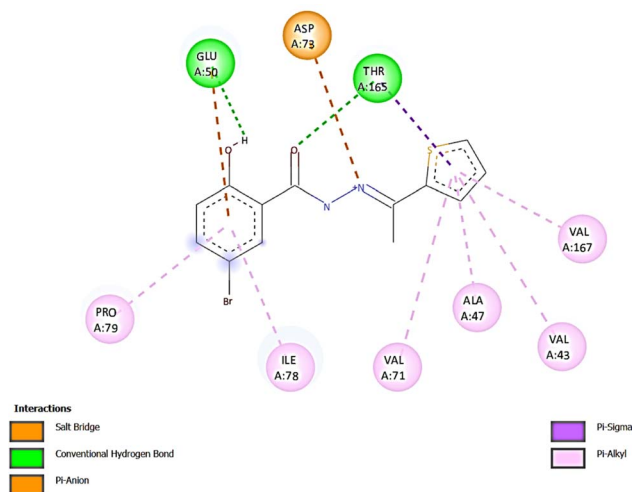

Fig. 9 2D diagram for the interaction mode of **L** with amino acid residues of *E. coli* DNA gyrase (PDB ID: 1 KZN).

3.7. Computational analysis of frontier molecular orbitals

To get an insight into the change of the energy gap of **L** before or after interaction with metal ions, we carried out the quantum mechanical calculations of the free probe and its metal coordinated complexes with the help of the DFT method using a Gaussian 09 program at the level of B3LYP/6-311G(d)/LANL2DZ for C, H, N, S, O, and metal ions, where for the complexes multiplicity were 2.

The frontier molecular orbitals provided effective information about electronic transitions, reactivity, biological activity,
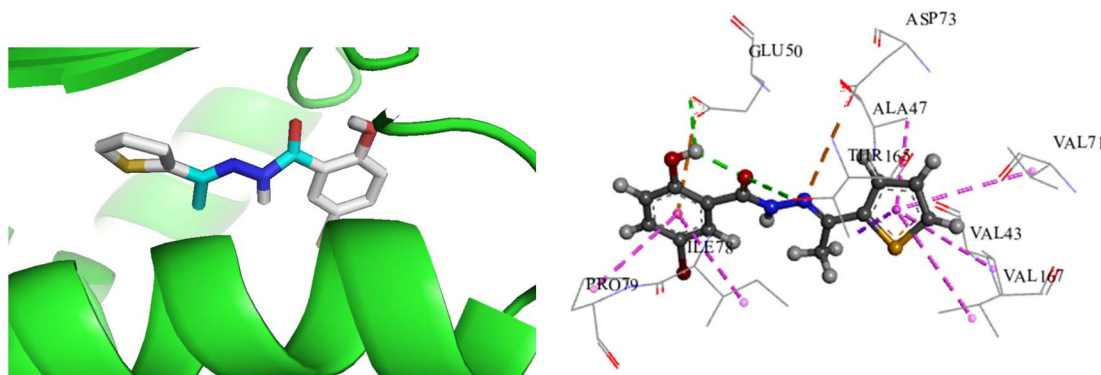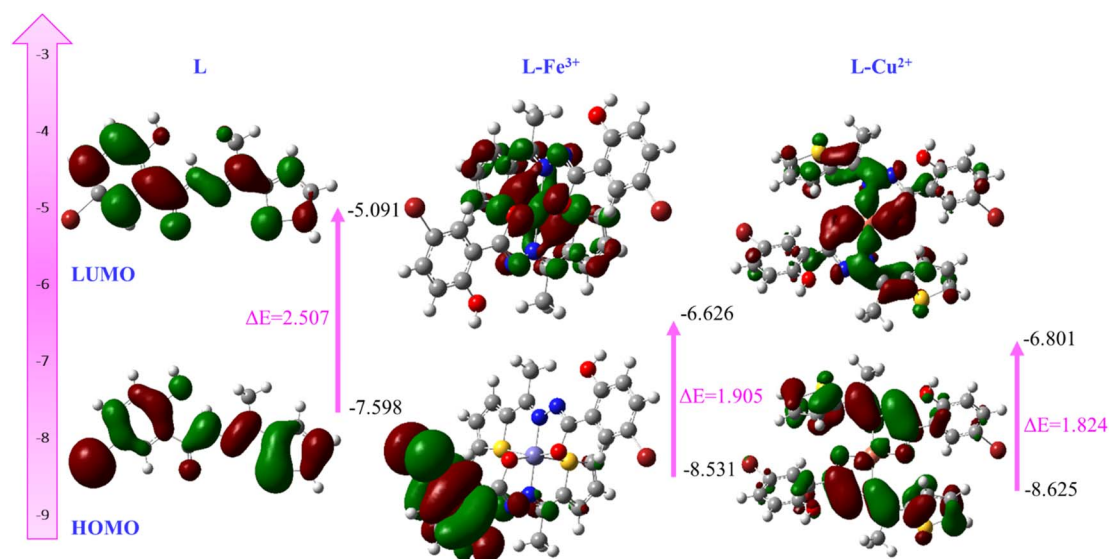

Fig. 8 Binding mode of **L** docked with *E. coli* DNA gyrase (PDB ID: 1 KZN); [green: H-bond, pink: hydrophobic interactions].

Table 3 Calculated binding energies and H-bond count of L in the active site of *E. coli* DNA Gyrase (PDB ID: 1KZN)

System	Binding energy (kcal mol^{-1})	L-Protein interaction			Other interacting residues (distance)
		No of H-bond	Amino acid residues	Distance (Å)	
L-1KZN	−7.7	2	GLU50 THR165	2.63 3.00	THR165 (3.75 Å), GLU50 (4.23 Å), VAL43 (4.62 Å), PRO79 (4.82 Å), VAL167 (5.06 Å), ILE78 (5.07 Å), ALA47 (5.43 Å), VAL71 (5.47 Å)

Fig. 10 Frontier molecular orbitals of L, L-Fe^{3+} and L-Cu^{2+} generated by B3LYP/6311G(d)/LANL2DZ.

and kinetic stability of **L** as well as metal complexes of Fe^{3+} and Cu^{2+}.[40–43] The highest occupied molecular orbital (HOMO) and lowest unoccupied molecular orbital (LUMO) of **L** were located within mostly on the whole π-moiety of thiophene as well as the –CO–NHN=CH– moiety with a HOMO–LUMO gap of 2.507 eV, which indicated the transition of π to π* of the thiophene unit. As evident from UV-visible and fluorescence titration spectra, the stoichiometry of **L** with Fe^{3+} and Cu^{2+} were confirmed strongly as 2 : 1 and hence, the optimization of the metal complex was carried out with 2 : 1 coordinated complexes. In the **L**-Fe^{3+} complex, the HOMO is situated completely on the whole ligand **L**, whereas LUMO is concentrated over Fe^{3+} ions with a band gap of 1.095 eV (Fig. 10). These results clearly revealed the interruption of internal charge transfer after the addition of Fe^{3+} ions to **L**. Similarly, the calculated HOMO–LUMO gap of Cu^{2+} complex was small compared to that of **L**. These findings intensely supported the reason for the colorimetric response upon the addition of metal ions Cu^{2+} to **L**.

Moreover, Snyder *et al.* reported that the smaller energy gap between HOMO and LUMO is a pivotal determinant to predict drug–receptor interactions and their electronic configuration.[44] Thus, the smaller energy gap of **L** supports antimicrobial activity.

4. Conclusion

In summary, a novel hydrazide–hydrazone-based chemosensor has been synthesized and characterized successfully by FT-IR, ^{1}H and ^{13}C NMR and mass spectroscopy. The antimicrobial assay revealed significant inhibition of **L** against *E. coli* Gram-negative bacteria. Fluorescence studies revealed that there was an enhanced fluorescence in the emission spectra, upon the addition of Fe^{3+} ions and that makes **L** a potential ratio metric as well as fluorescence turn-on chemosensor, which was strongly supported by the elevating quantum yields. Further, the novel sensor exhibited colorimetric responses with significant color change from colorless to yellow toward biologically important metal ion Cu^{2+} in DMSO over other metal cations ions (Cr^{3+}, Mn^{2+}, Pb^{2+}, Fe^{2+}, Fe^{3+}, Co^{2+}, Ni^{2+}, Zn^{2+}, Mg^{2+}, Ca^{2+}, Al^{3+} and Bi^{2+}). That's why **L** can act as an excellent chemosensor for the detection of Cu^{2+} in the environment. Also, **L** may be applied for the detection of biologically important metal ion Fe^{3+} in the bioimaging of live cells. Thus, due to the wide application of such hydrazide–hydrazone compounds and their simple, low-cost synthetic procedure, such compounds can be a target for drug design.

Author contributions

Conflicts of interest

The authors declare no competing financial interest.

Acknowledgements

References

1 S. A. Rupa, M. R. Moni, M. A. M. Patwary, M. M. Mahmud, M. A. Haque, J. Uddin and S. M. T. Abedin, Synthesis of Novel Tritopic Hydrazone Ligands: Spectroscopy, Biological Activity, DFT, and Molecular Docking Studies, *Molecules*, 2022, **27**, 1656, DOI: 10.3390/molecules27051656.

2 R. Anbazhagan and K. R. Sankaran, Design, synthesis, computational calculation and biological evaluation of some novel 2-thiazolyl hydrazones, *Spectrochim. Acta, Part A*, 2015, **135**, 984–993.

3 G. R. Kaki, B. Sreenivasulu, A. Islam, D. Nageshwar, R. Korupolu and B. V. Rao, Synthesis, characterization, and antimicrobial activity of hydrazone derivatives of 2-(2,3-dihydrobenzofuran-5yl)acetic acid, *J. Appl. Chem.*, 2014, **3**(4), 1481–1487.

4 L. Popiołek and A. Biernasiuk, Synthesis and investigation of antimicrobial activities of nitrofurazone analogues containing hydrazide-hydrazone moiety, *Saudi Pharm. J.*, 2017, **25**, 1097–1102.

5 G. L. Backes, D. M. Neumann and B. S. Jursic, Synthesis and antifungal activity of substituted salicylaldehyde hydrazones, hydrazides and sulfohydrazides, *Bioorg. Med. Chem.*, 2014, **22**, 4629–4636.

6 N. Terzioglu and A. Gürsoy, Synthesis and anticancer evaluation of some new hydrazone derivatives of 2,6-dimethylimidazo[2,1-*b*][1,3,4]thiadiazole-5-carbohydrazide, *Eur. J. Med. Chem.*, 2003, **38**(7–8), 781–786.

7 O. A. Nurkenov, Z. H. B. Satpaeva, I. A. Schepetkin, A. I. Khlebnikov, K. M. Turdybekov, T. M. Seilkhanov and S. D. Fazylov, Synthesis and biological activity of hydrazones of o- and p-hydroxybenzoic acids. Spatial structure of 5-bromo-2-hydroxybenzylidene-4-hydroxybenzohydrazide, *Russ. J. Gen. Chem.*, 2017, **87**, 2299–2306.

8 Z. Moussa, M. Al-Mamary, S. Al-Juhani and S. A. Ahmed, Preparation and biological assessment of some aromatic hydrazones derived from hydrazides of phenolic acids and aromatic aldehydes, *Heliyon*, 2020, **6**(6), e05019.

9 F. Rahim, H. Ullah, M. Taha, A. Wadood, M. T. Javed, W. Rehman, M. Nawaz, M. Ashraf, M. Ali, M. Sajid, F. Ali, M. N. Khan and K. M. Khan, Synthesis and *in vitro* acetylcholinesterase and butyrylcholinesterase inhibitory potential of hydrazide-based Schiff bases, *Bioorg. Chem.*, 2016, **68**, 30–40.

10 S. A. Rupa, W. E. Ghann, M. A. M. Patwary and J. Uddin, Highly selective naked eye Pyridine-2,6-dicarbohydrazide based colorimetric and fluorescence chemosensor for Pb^{2+} with AIE activity, *Inorg. Chem. Commun.*, 2022, **144**, 109937.

11 S. Sharma, G. Dubey, B. S. Sran, P. V. Bharatam and G. Hundal, Fabrication of a Hydrazone-Based Al(III)-Selective "Turn-On" Fluorescent Chemosensor and Ensuing Potential Recognition of Picric Acid, *ACS Omega*, 2019, **4**, 18520–18529.

12 C. A. S. Pothulapadu, A. Jayaraj, N. Swathi, R. N. Priyanka and G. Sivaraman, Novel Benzothiazole-Based Highly Selective Ratiometric Fluorescent Turn-On Sensors for Zn^{2+} and Colorimetric Chemosensors for Zn^{2+}, Cu^{2+}, and Ni^{2+} Ions, *ACS Omega*, 2021, **6**, 24473–24483, DOI: 10.1021/acsomega.1c02855.

13 K. P. Carter, A. M. Young and A. E. Palmer, Fluorescent sensors for measuring metal ions in living systems, *Chem. Rev.*, 2014, **114**, 4564–4601.

14 J. H. Xu, Y. M. Hou, Q. J. Ma, X. F. Wu and X. J. Wei, A highly selective fluorescent sensor for Fe^{3+} based on covalently immobilized derivative of naphthalimide, *Spectrochim. Acta, Part A*, 2013, **112**, 116–124, DOI: 10.1016/j.saa.2013.04.044.

15 S. Sasan, T. Chopra, A. Gupta, D. Tsering, K. K. Kapoor and R. Parkesh, Fluorescence "Turn-Off" and Colorimetric Sensor for Fe^{2+}, Fe^{3+}, and Cu^{2+} Ions Based on a 2,5,7-Triarylimidazopyridine Scaffold, *ACS Omega*, 2022, **7**(13), 11114–11125.

16 H. Ebrahimi, P.-L. Hagedoorn and W. R. Hagen, Unity in the Biochemistry of the Iron-Storage Proteins Ferritin and Bacterioferritin Kourosh, *Chem. Rev.*, 2015, **115**, 295–326.

17 M. B. Zimmermann and R. F. Hurrell, Nutritional iron deficiency, *Lancet*, 2007, **370**, 511–520, DOI: 10.1016/S0140-6736(07)61235-5.

18 M. G. Savelieff, G. Nam, J. Kang, H. J. Lee, M. Lee and M. H. Lim, Development of Multifunctional Molecules as Potential Therapeutic Candidates for Alzheimer's Disease, Parkinson's Disease, and Amyotrophic Lateral Sclerosis in

the Last Decade, *Chem. Rev.*, 2019, **119**, 1221–1322, DOI: 10.1021/acs.chemrev.8b00138.

19 J. Zhao, Y.-y. Wang, W.-l. Chen, G.-s. Hao, J.-p. Sun, Q.-f. Shi, F. Tian and R.-t. Ma, A salicylaldehyde benzoyl hydrazone-based near-infrared probe for copper(ii) and its bioimaging applications, *RSC Adv.*, 2022, **12**, 3073–3080.

20 S. Mukherjee and S. Betal, Sensing phenomena, extraction and recovery of Cu^{2+} followed by smartphone application using a luminescent pyrene based chemosensor, *J. Lumin.*, 2018, **204**, 145–153, DOI: 10.1016/j.jlumin.2018.07.038.

21 S. Wasi, S. Tabrez and M. Ahmad, Toxicological effects of major environmental pollutants: an overview, *Environ. Monit. Assess.*, 2013, **185**, 2585–2593.

22 M. Khalaj, M. Kamali and Z. Khodaparast, Copper-based nanomaterials for environmental decontamination – An overview on technical and toxicological aspects, *Ecotoxicol. Environ. Saf.*, 2018, **148**, 813–824.

23 S. G. Kaler, ATP7A-related copper transport diseases emerging concepts and future trends, *Nat. Rev. Neurol.*, 2011, **7**, 15–29.

24 R. Dwivedi, S. Singh, B. S. Chauhan, S. Srikrishna, A. K. Panday, L. H. Choudhury and V. P. Singh, Aroyl hydrazone with large Stokes shift as a fluorescent probe for detection of Cu^{2+} in pure aqueous medium and *in vivo* studies, *J. Photochem. Photobiol., A*, 2020, **395**, 112501.

25 N. Guex and M. C. Peitsch, SWISS-MODEL and the Swiss-PdbViewer: an environment for comparative protein modeling, *Electrophoresis*, 1997, **18**(15), 2714–2723.

26 W. DeLano, *The PyMOL Molecular Graphics System*, 2002.

27 S. Dallakyan and A. J. Olson, Small-molecule library screening by docking with PyRx, *Methods Mol. Biol.*, 2015, **1263**, 243–250.

28 Accelrys Software Inc., *Discovery Studio Modeling Environment, Release 4.0*, San Diego, Accelrys Software Inc., 2013.

29 V. M. Chaitali and D. Jayashree, Review of heavy metals in drinking water and their effect on human health, *Int. J. Innov. Res. Sci., Eng. Technol.*, 2013, **7**, 2992–2996.

30 A. Roy, U. Shee, A. Mukherjee, S. K. Mandal and P. Roy, Rhodamine-based dual chemosensor for Al^{3+} and Zn^{2+} ions with distinctly separated excitation and emission wavelengths, *ACS Omega*, 2019, **4**, 6864–6875.

31 R. Dwivedi, D. P. Singh, B. S. Chauhan, S. Srikrishna, A. K. Panday, L. H. Choudhury and V. P. Singh, Intracellular application and logic gate behavior of a 'turn off-on-off' type probe for selective detection of Al^{3+} and F^- ions in pure aqueous medium, *Sens. Actuators, B*, 2018, **258**, 881–894.

32 P. Sathyadevi, P. Krishnamoorthy, R. R. Butorac, A. H. Cowley, N. S. P. Bhuvanesh and N. Dharmaraj, Effect of substitution and planarity of the ligand on DNA/BSA interaction, free radical scavenging and cytotoxicity of diamagnetic Ni (II) complexes: a systematic investigation, *Dalton Trans.*, 2011, **40**, 9690–9702.

33 Y. Dong, R. Fan, W. Chen, P. Wang and Y. Yang, A simple quinolone Schiff-base containing CHEF based fluorescence 'turn-on' chemosensor for distinguishing Zn^{2+} and Hg^{2+} with high sensitivity, selectivity and reversibility, *Dalton Trans.*, 2017, **46**, 6769–6775.

34 G. M. Khairy, A. S. Amin, S. M. N. Moalla, A. Medhat and H. Nader, Fluorescence determination of Fe(III) in drinking water using a new fluorescence chemosensor, *RSC Adv.*, 2022, **12**, 27679–27686.

35 F. Rahman, M. A. M. Patwary, M. A. B. Siddique, M. S. Bashar, M. A. Haque, B. Akter, R. Rashid, M. A. Haque and A. K. M. R. Uddin, Green synthesis of ZnO nanoparticles using Cocos nucifera leaf extract: Characterization, antimicrobial, antioxidant, and photocatalytic activity, *R. Soc. Open Sci.*, 2022, **9**, 220858, DOI: 10.1098/rsos.220858.

36 A. F. M. Sanaullah, P. Devi, T. Hossain, S. B. Sultan, M. M. U. Badhon, M. E. Hossain, J. Uddin, M. A. M. Patwary, M. Kazi and M. M. Matin, Rhamnopyranoside-Based Fatty Acid Esters as Antimicrobials: Synthesis, Spectral Characterization, PASS, Antimicrobial, and Molecular Docking Studies, *Molecules*, 2023, **28**(3), 986, DOI: 10.3390/molecules28030986.

37 S. Saranya, J. Haribabu, V. N. V. Palakkeezhillam, P. Jerome, K. Gomathi, K. K. Rao, V. H. H. S. Babu, R. Karvembu and D. Gayathri, Molecular structures, Hirshfeld analysis and biological investigations of isatin based thiosemicarbazones, *J. Mol. Struct.*, 2019, **1198**, 126904.

38 S. Murugavel, S. Deepa, C. Ravikumar, R. Ranganathan and R. P. Alagusundaram, Synthesis, structural, spectral and antibacterial activity of 3,3a,4,5-tetrahydro-2*H*-benzo[g] indazole fused carbothioamide derivatives as antibacterial agents, *J. Mol. Struct.*, 2020, **1222**, 128961, DOI: 10.1016/j.molstruc.2020.128961.

39 S. Deswal, Naveen, R. K. Tittal, D. G. Vikas, K. Lal and A. Kumar, 5-Fluoro-1H-indole-2,3-dione-triazoles-synthesis, biological activity, molecular docking, and DFT study, *J. Mol. Struct.*, 2020, **1209**, 127982.

40 V. N. V. Palakkeezhillam, J. Haribabu, V. Manakkadan, P. Rasin, R. Varughese, D. Gayathri, N. Bhuvanesh, C. Echeverria and A. Sreekanth, Synthesis, spectroscopic characterizations, single crystal X-ray analysis, DFT calculations, *in vitro* biological evaluation and *in silico* evaluation studies of thiosemicarbazones based 1,3,4-thiadiazoles, *J. Mol. Struct.*, 2023, **1273**, 134309.

41 P. Rasin, V. Manakkadan, V. N. V. Palakkeezhillam, J. Haribabu, C. Echeverria and A. Sreekanth, Simple Fluorescence Sensing Approach for Selective Detection of Fe^{3+} Ions: Live-Cell Imaging and Logic Gate Functioning, *ACS Omega*, 2022, **7**, 33248–33257.

42 C. Arivazhagan, R. Borthakur and S. Ghosh, Ferrocene and Triazole-Appended Rhodamine Based Multisignaling Sensors for Hg^{2+} and Their Application in Live Cell Imaging, *Organometallics*, 2015, **34**, 1147–1155.

43 C. Arivazhagan, R. Borthakur, R. Jagana and S. Ghosh, Benzoindolium–triarylborane conjugates: a ratiometric fluorescent chemodosimeter for the detection of cyanide ions in aqueous medium, *Dalton Trans.*, 2016, **45**, 5014–5020.

44 E. J. Lien, Z. R. Guo, R. Li and C. T. Su, Use of dipole moment as a parameter in drug-receptor interaction and quantitative structure-activity relationship studies, *J. Pharm. Sci.*, 1982, **71**, 641–655.